Proceedings of IMECE2005
2005 ASME International Mechanical Engineering Congress and Exposition
November 5-11, 2005, Orlando, Florida USA

IMECE2005-80582

ACTIVE AND EVENT-DRIVEN PASSIVE MECHANICAL FAULT IDENTIFICATION IN GROUND VEHICLE SUSPENSION SYSTEMS

Muhammad Haroon
Purdue University
School of Mechanical Engineering
Ray W. Herrick Laboratories
140 S. Intramural Drive
West Lafayette, Indiana 47907-2031
(765)494-0231
(765)494-0787
mharoon@purdue.edu

Douglas E. Adams
Purdue University
School of Mechanical Engineering
Ray W. Herrick Laboratories
140 S. Intramural Drive
West Lafayette, Indiana 47907-2031
(765)496-6033
(765)494-0787
deadams@purdue.edu

ABSTRACT

Data interrogation methodologies are needed for identifying loads and faults in suspensions, tires, and other vehicle components to help design more durable systems and reduce the total cost of ownership. The application of passive and active data interrogation methodologies to passenger vehicle suspension systems is discussed here.

For passive diagnostics, operating acceleration response data in conjunction with fundamental mechanics models are utilized. Mechanical faults in suspension components, e.g. degradation to shock, are identified using force state maps and transmissibility functions. First, it is shown that damage causes changes in the frequency characteristics of restoring forces, provided by the force state maps, which help to detect damage. Second, autoregressive nonlinear transmissibility models are used to locate faults and also characterize the degree to which faults alter nonlinear correlations in the response data. Force state maps are suited to narrow band inputs (e.g., sinusoidal) and transmissibility models are suited to broad-band inputs (e.g., random). This difference in preferential bandwidth for the two different data analysis methods motivates the selection of the diagnostic algorithm in an event-driven manner.

For active diagnostics, experimental sensitivity functions, which are algebraic combinations of measured frequency response data, estimate the change in the forced response of the system with perturbation in stiffness or damping. By comparing the sensitivity functions to finite difference functions, faults can be detected, located, and quantified. The passive and active techniques are applied to experimental vehicle data and various issues (e.g., quantifying faults) are discussed.

NOMENCLATURE

C	Damping
K	Stiffness
M	Mass
MDOF	Multiple degrees of freedom
$A(\omega)$	Auto-regressive coefficient
$B(\omega)$	Exogenous coefficient
$F(\omega)$	Fourier transform of the measured force history
$H_{jk}(\omega)$	Frequency response function (FRF) between j and k
K_{mn}	Stiffness between m and n
$N_k[x_1(t), x_2(t), \dot{x}_1(t)\dot{x}_2(t)]$	Nonlinear forces
$\Re_i$	Set of Real numbers
$X(j\omega), Y(k)$	Fourier transform of measured time history
$\ddot{x}(t)$	Measured acceleration time history
j,k,m,n	Degrees of freedom

1 INTRODUCTION

There is a trend in the automotive industry towards the manufacture of integrated suspension systems in contrast to the historical approach where suspension components supplied by different manufacturers were assembled. The benefit is that integrated modules manufactured by one company, with design authority over all interconnected components, have higher performance and last longer. Integrated suspension modules incorporate subsystems including shock absorbers, struts, torsion bars, mounts, etc., leading to complex loading and degradation mechanisms. These loads and forms of degradation lead to anticipated and unanticipated failure mechanisms in components and subsystems. The consequences of degradation are

undue warranty costs and overly aggressive maintenance schedules, which both lead to increased cost of vehicle ownership. These high costs warrant the development of data interrogation methodologies to identify loads and faults in vehicle suspensions (e.g., bushing rupture, joint preload, leaky shock, warped torsion bar). This information in turn will help to design more durable suspension systems.

Various vibration-based damage identification techniques have been developed. Doebling et al. [1,2] presented a literature review of methods based on changes in the vibration characteristics of mechanical systems. This paper presents three such vibrations-based methods.

Rytter [3] defines four levels of damage identification, as follows:

- Level 1: Determination that damage is present in the structure.
- Level 2: Level 1 plus the determination of the geometric location of the damage.
- Level 3: Level 2 plus quantification of the severity of the damage.
- Level 4: Level 3 plus prediction of the remaining service life of the structure.

The techniques presented here work up to level three, i.e. detect, locate and quantify damage. Both passive and active data interrogation methodologies are utilized. The passive methods utilize response acceleration data along with fundamental mechanics models. One passive method is the restoring force technique, which was presented by Masri et al. [4,5], who used recursive least squares for linear parameter identification and a non-parametric method for expressing the nonlinear characteristics in terms of orthogonal functions. Haroon et al. [6] extended the technique to nonlinear characterization and system identification of mechanical systems in the absence of an input measurement. In this paper, the restoring force technique is used to characterize the internal forces in the components of a ground vehicle suspension system and to identify damage using changes in the internal forces caused by degradation. This technique is more suited to narrow-band inputs (e.g., sinusoidal).

The second passive technique is based on the Discrete Frequency Domain Models presented by Adams and Allemang [7]. Adams [8] used these models to develop frequency domain auto-regressive exogenous input (ARX) models, which relate the response of a nonlinear system to the input and output at harmonics of the forcing frequency. These harmonic relationships indicate that the response of a nonlinear vibrating system at a particular frequency, ω_k, $X(\omega_k)$, is correlated with both the input(s) at that frequency, $F(\omega_k)$, and the response at sub and super-harmonics of that frequency, $X(\omega_{k-i})$ and $X(\omega_{k+i})$. Adams and Farrar [9] applied frequency domain ARX models to damage identification. They developed features that can be used to detect changes in the linear and nonlinear behavior of structural systems with the onset of damage. Similar models are used here to detect and follow the progress of damage in a ground vehicle suspension system. When the transmissibility version of the ARX models is used, they can help to detect and locate damage. The reason for this dual capability is that transmissibility functions contain only the transmission zeros of the system and, hence, are sensitive to local changes in system characteristics [10,11]. This technique is more suited to broad-band inputs (e.g., random).

The preferential frequency bandwidth of the two passive algorithms means that either of the two algorithms can be chosen in an event-driven manner. If the response measurements have narrowband frequency content, restoring forces can be used and if the frequency content is broadband, ARX (transmissibility function) models can be used. This frequency bandwidth requirement of these and other diagnostic algorithms can be used to select the algorithm best suited for a particular observed/measured response, hence, the term event-driven.

The active technique uses experimental sensitivity functions developed by Yang et al. [12]. The technique involves experimentally estimating the sensitivity of a given vibration phenomenon to a system component parameter (mass, damping, stiffness). The sensitivity functions are algebraic combinations of measured frequency response function (FRF) data that determine how the forced responses of a structure change with perturbations in mass, damping, and stiffness. Johnson et al. [13] showed that these sensitivity functions can be used to detect, locate and quantify damage. By comparing the sensitivity functions with finite difference functions, level 3 damage identification can be performed. In this paper, experimental sensitivity functions are used to detect damage in a vehicle suspension system. In the absence of a force measurement, a fundamental mechanics model is used to estimate the force input to the spindle (unsprung mass) from the tire, using acceleration measurements at the tire patch.

In the following sections, the three techniques described above are explained in more detail and then applied to experimental vehicle data with simulated damage.

2 FRAMEWORK

2.1 Passive Techniques

2.1.1 Restoring Force. The restoring force is an internal force that opposes the motion of an inertial element within a system, i.e., the left hand side of Newton's Second Law for a body with constant mass, m, and acceleration vector, a: $\Sigma F = ma$. The stiffness and damping in a system resist the motion of a given inertia; consequently, the forces in the stiffness and damping elements are referred to as components of the restoring forces.

The chief advantage of the restoring force technique is that it only requires that the output accelerations of a system be measured. Consider the two degree-of-freedom quarter car model shown in Fig. 1. The equation for the sprung mass, M_2, can be written using Newton's Second Law to give the following expression for the restoring force in the suspension:

$$M_2\ddot{x}_2 = -C_2(\dot{x}_2 - \dot{x}_1) - K_2(x_2 - x_1) - K_3 x_2 + N_1[x_1(t), x_2(t), \dot{x}_1(t), \dot{x}_2(t)] \quad (1)$$

The relationships in the form of plots between the acceleration of the sprung mass and the relative velocity or the relative displacement between the sprung mass and the unsprung mass allow the damping or stiffness restoring force, respectively, in the suspension to be estimated. There are two main features of restoring forces that make them suitable for damage detection:

1) Restoring forces are determined by the damping and stiffness (linear or nonlinear) of a system. Structural damage often causes changes in these system parameters and, consequently, the restoring forces.
2) Individual nonlinearities have distinct restoring forces and damage causes changes in the nonlinear characteristics, which can be indictors of damage.

For example, Fig. 2 shows the damping and stiffness restoring force plots for a particular input amplitude and frequency showing the damping and stiffness nonlinearities observed in the strut of a suspension system of an experimental vehicle test bed. These plots illustrate the nature of nonlinear restoring forces. The frequency dependent nature of restoring forces dictate that the inputs be narrowband so that the characteristics, and changes in those characteristics, can be observed at particular discrete frequencies. Note that in experimental data analysis, acceleration measurements are the most convenient measurements to make and can also be integrated to estimate velocity and displacement time histories; therefore, restoring force methods are especially appropriate for experimental purposes.

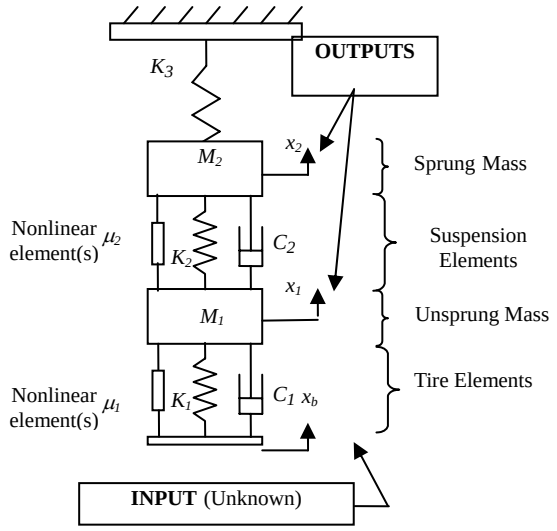

Fig 1: Quarter car model.

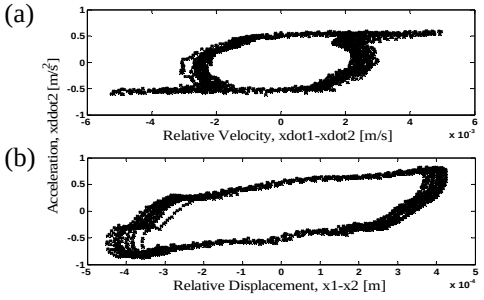

Fig 2: (a) Nonlinear shock damping showing saturation at a certain relative clearance velocity (Frequency 4.12 Hz) and (b) nonlinear hysteretic stiffness showing backlash characteristic (Frequency 4.5 Hz.); Input amplitude 0.5 mm.

2.1.2 Frequency Domain Nonlinear ARX Models. The models, based on discrete frequency models (DFMs) developed in [7] and applied in [8,9], take the form

$$Y(k) = B(k)U(k) + \sum_{r,s \in \Re_i} A_{r,s}(k) \times f_{r,s}\left(Y\left(\frac{p_r}{q_r}k\right), Y\left(\frac{p_s}{q_s}k\right)\right) \quad (2)$$

where k, r, s, $(p_r/q_r)k$, and $(p_s/q_s)k$ are contained in $\Re_i$, k is a simple frequency counter, $U(k)$ is the input, and $B(k)$ and $A_{r,s}(k)$ are complex frequency coefficients. The first term is the exogenous component, which accounts for the nominal linear dynamics and the second term is the auto-regressive (AG) component, which accounts for the nonlinear frequency correlations. The rational number arguments, $(p_r/q_r)k$, are used to represent different harmonics of the excitation frequency. As stated earlier, Eq. (2) indicates that the harmonic response of a nonlinear system at each frequency is correlated with both the input and response at potentially all the harmonics of the input frequency. This multidimensional correlation is due to nonlinear feedback in the system.

When the functions $f_{r,s}(.)$ are linear, they indicate in what frequency ranges the nonlinearity dominates but may not describe all of the nonlinear dependencies of the response on the input. Hence, Eq. (2) is a data model. When the $f_{r,s}(.)$ are nonlinear functions of the harmonics of the spectrum, $Y(k)$, then the model can more fully describe different types of nonlinear behavior. In summary, the $f_{r,s}(.)$ determine the degree to which the nonlinear frequency domain ARX model is able to describe the behavior of the nonlinear system.

As these models use frequency spectra of measured signals, and spectra are easier to obtain from signals with broad frequency content, this technique is suited to broad-band inputs (e.g., random).

Equation (2) can be written as,

$$Y(k) = Dp \quad (3)$$

where p are the exogenous and auto-regressive coefficients and D contains the input and the terms $f_{r,s}(.)$. The optimum set of ARX coefficients, the ones that minimize the sum of the squared error, $e(k).e(k)$, is given by the pseudo-inverse solution, $\hat{p}$, to the over-determined Eq. (3):

$$\hat{p} = D^{+}Y(k) = (D^T D)^{-1} D^T Y(k) \quad (4)$$

where D^{+} is the pseudo-inverse of D and D^T is the transpose.

The order of the nonlinear ARX model is determined by the number of auto-regressive (AG) terms that are included in the function $f_{r,s}(.)$, on one side of the frequency of interest, ω_k. Two forms of the ARX model are used in this paper.

1st Order, Linear:

$$Y(k) = B(k)U(k) + \sum_{j=-1\neq 0}^{1} A_j(k)Y(k-j) \quad (5)$$

1st Order, Nonlinear:

$$Y(k) = B(k)U(k) + A_{-1}(k)Y^3\left(\frac{k}{3}\right) + A_1(k)Y^3(3k) \tag{6}$$

Equation (2) can easily be adapted for passive data (output-only) by using the transmissibility function formulation, where a measured output at a location different than that for *Y(k)* is used as the input term, *U(k)*.

The changes in the exogenous coefficients (related to nominally linear behavior) and auto-regressive coefficients (related to nonlinear behavior) can be used as indicators of damage, as damage causes changes in the linear/nonlinear behavior of a structural system. A number of other indicators can be used that signify the onset and progression of damage in a system. The features used in this paper are $1-\left|A_j(\omega)\right|$, which are like ordinary coherence functions, and $1-\left|A_{j_d} \middle/ A_{j_{un}}\right|$, where *'d'* indicates damaged and *'un'* indicates undamaged.

As stated earlier, the preferential bandwidth of the two passive techniques discussed here suggests that the selection of the diagnostic algorithm can be made on the basis of the frequency bandwidth of measured system response. Restoring forces can be used for narrowband response and ARX models can be used for broadband response.

2.1.3 Limitations. The passive nature of the techniques means that there is no guarantee that the excitations are persistent enough to accentuate the damage, and as such small defects may be harder to find. In addition, the low frequency range inhibits the detection of small, incipient damage which is better accentuated by high frequency excitations. Quantification of faults is also difficult with these methods. Restoring forces, based on lumped parameter models, do not work well for structures which do not have discrete connecting parts, for example plates and shells.

2.2 Active Technique

2.2.1 Experimental Sensitivity Functions. Experimental sensitivity functions as defined by Yang et al. [12] are the partial derivatives of FRFs with respect to lumped system parameters (mass, damping or stiffness) as a function of frequency. The formula for calculating sensitivities in general multiple-degree-of-freedom (MDOF) linear systems was derived in this earlier work.

$$\frac{\partial H_{jk}(\omega)}{\partial K_{mn}} = -\left[H_{jm}(\omega) - H_{jn}(\omega)\right]\left[H_{km}(\omega) - H_{kn}(\omega)\right] \tag{7a}$$

$$\frac{\partial H_{jk}(\omega)}{\partial C_{mn}} = j\omega\frac{\partial H_{jk}(\omega)}{\partial K_{mn}} \tag{7b}$$

$$\frac{\partial H_{jk}(\omega)}{\partial M_{m0}} = (j\omega)^2\frac{\partial H_{jk}(\omega)}{\partial K_{m0}} \tag{7c}$$

where

$$H_{j0}(\omega) = 0 \tag{7d}$$

Equations (7b) and (7c) are just frequency multiples of Eq. (7a). In Eq. (7a), H_{jk} is the FRF between the input force degree-of-freedom (DOF) k and output response DOF j and K_{mn} is the stiffness element between DOF m and n. DOF 0 (zero) denotes a boundary condition. The right-hand side of Eq. (7a) is a function of four potentially different FRFs. The worth of the formulae in Eqs. (7a)-(7c) is that as each sensitivity can be calculated directly from FRFs, which are computed from measured data, full analytical models of a given structure are not needed because specific values of structural parameters are not required.

Structural damage is often characterized by a change in one or more of the system parameters. These changes cause changes in the system FRFs, which can be compared to the experimental sensitivities of the baseline (healthy) system to determine which system parameter(s) caused the FRF to change. Johnson et al. [13] showed that experimental sensitivities also provide an absolute quantity of the change in the system parameters, by taking the ratio of the change in the system FRF with respect to the experimental sensitivity function corresponding to damage (change in stiffness, damping or mass). The variation in the FRF is approximated by a finite difference and, hence, is only accurate if the changes in the FRFs are relatively small. For small changes in the measured FRF, $\Delta H_{jk}(\omega)$, the corresponding change in stiffness is given by

$$\Delta K_{mn} \approx \frac{\Delta H_{jk}(\omega)}{\left(\partial H_{jk}(\omega)/\partial K_{mn}\right)} = \frac{\Delta H_{jk}(\omega)}{-\left[H_{jm}(\omega) - H_{jn}(\omega)\right]\left[H_{km}(\omega) - H_{kn}(\omega)\right]} \tag{8a}$$

where

$$\Delta H_{jk}(\omega) = H_{jk}(\omega)\big|_{damaged} - H_{jk}(\omega)\big|_{undamaged} \tag{8b}$$

Changes in damping or mass can be estimated in a similar manner.

The procedure for applying experimental sensitivity functions for continuous structural health monitoring (SHM) was described by Johnson et al. [13]. In this paper, the sensitivity functions are used to identify simulated damage to a vehicle suspension system and quantify the change in a system parameter associated with the particular damage scenario.

2.2.2 Limitations. A measurement of input force is required, which is difficult in many cases. Many nonlinear damage mechanisms, for example cracks, cannot be described by a local reduction in linear parameters, which makes such damage difficult to quantify. As the method is based on a finite difference approximation of the variation in the system FRFs, accurate estimates of stiffness, damping or mass reduction can only be obtained if the changes in the measured FRFs are small. The sensitivity of FRFs to global changes in structural parameters means this technique is not well-suited for cases with multiple damage locations.

3 EXPERIMENTAL DATA ANALYSIS

The damage identification techniques presented in the previous section are applied to data from laboratory experiments on a full vehicle in this section.

3.1 Experimental Setup

Response data were taken on the front left suspension system of an Isuzu Impulse and a Lexus ES330 using a hydraulic shaker apparatus. A picture of the experimental setup is shown in Fig. 3. The MTS® hydraulic shaker, with a maximum dynamic pressure of 3000 psi, an input frequency range of 0-100 Hz and a maximum stroke of approximately 8 inches, was used to excite the tire patch of the car with different types of inputs in the vertical direction. Tri-axial accelerometers of nominal sensitivity 1 V/g were attached at five locations on the suspension system, (a) bottom of the strut, $\ddot{x}_1(t)$ (unsprung mass), (b) the upper strut connection with the body, $\ddot{x}_2(t)$, (sprung mass) (c) steering knuckle-control arm connection, $\ddot{x}_3(t)$, (d) control arm, $\ddot{x}_4(t)$ and (e) sway bar, $\ddot{x}_5(t)$. It should be noted that the actual system has more DOF than the model in Fig. 1. Damage was introduced in the suspension system of both cars by loosening the bolt connecting the steering knuckle to the control arm, through a ball joint.

Fig 3: Shaker testing setup.

The acceleration signals were recorded with an IOTech® Portable Data Acquisition System and converted into '.mat' files for further analysis in MATLAB®. The IOTech® system allowed a wide range of sampling frequencies and the application of high and/or low pass filters to remove noise and aliasing.

3.2 Restoring Forces

As mentioned before, restoring forces are easier to generate from narrowband responses. Hence, a very slow chirp input from 0-15 Hz, at a rate of 0.025 Hz/s, was used as the base excitation to the tire patch of the Isuzu. The acceleration response measurements were taken and then integrated offline to estimate the velocity and displacement responses. The signal processing parameters that were used are given in Tab. 1. A 100 Hz bandwidth low pass filter was used to reduce aliasing back into the frequency range of interest from approximately 3 to 35 Hz.

Table 1: Signal Processing Parameters for the Chirp Input.

Chirp Range (Hz)	Chirp Rate (Hz/s)	Number of time points, N_t	Sampling Frequency, F_s (Hz)	Low pass filter (LPF) cut-off (Hz)
0-15	0.025	360,000	600	100

Velocity (damping) and displacement (stiffness) restoring force curves were generated for different input amplitudes and frequencies, for the damaged and undamaged cases. Figure 2 shows two representative restoring force curves, in the vertical direction, for an input amplitude of 0.5 mm. The first curve, Fig. 2(a), shows the sprung mass acceleration versus the velocity difference between the unsprung and sprung mass and the second curve, Fig. 2(b), is a function of the displacement difference. The velocity curve (Fig. 2(a)) shows a nonlinear damping characteristic with both saturation (Coulomb friction damping curve) and hysteresis. The displacement curve (Fig. 2(b)) shows a nonlinear stiffness characteristic with primarily hysterisis (i.e., backlash). These two types of nonlinearities are present to varying degrees across the entire amplitude and frequency range.

The bolt connecting the steering knuckle to the control arm (Fig. 4) was loosened from an initial torque of 400 lb-in to 250 lb-in, 100 lb-in and finally it was removed completely. Restoring force curves were generated for the different cases to study the change in the internal forces with progression of damage. Figure 5 shows the frequency characteristic of the vertical damping restoring force between points x_2 (body) and x_3 (steering knuckle-control arm), for the undamaged case (400 lb-in bolt torque). This path is dominated by the forces in the strut and also contains the damage induced by loosening of the bolt. The damping force initially has a central hysterisis loop, and as the frequency increases, the force takes on the shape of a Coulomb friction curve and eventually a piecewise-linear characteristic. Figure 6 shows the characteristic of the same internal force as the damage progresses (bolt loosened).

Fig 4: Damage location.

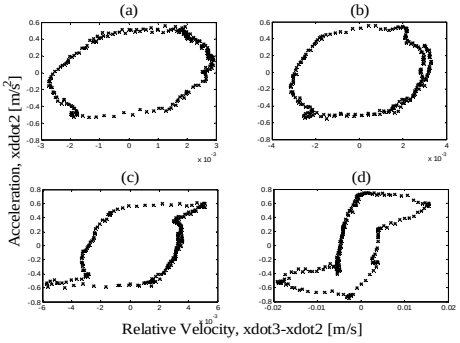

Fig 5: Frequency characteristic of damping internal force in the strut (a) 4.05 Hz, (b) 4.09 Hz, (c) 4.17 Hz and (d) 4.37 Hz. Input amplitude 0.5 mm.

Figure 6 shows that damage causes changes in the frequency characteristic of the damping internal force. The system moves out of the hysterisis loop at different frequencies because of the damage. The intermediate cases (loosened bolts) change characteristic at higher frequencies compared to the undamaged case and the most severe damage case (bolt removed) changes characteristic at a lower frequency. For example, in Figs. 5(a) and 6(a) at 4.05 Hz, the restoring force corresponding to the case with no bolt has already taken on the shape of a Coulomb friction curve while the restoring forces for the other three cases only show a hysterisis loop. The undamaged restoring force assumes the Coulomb friction form at a later frequency of 4.09 Hz and the loosened bolt cases do not take this form until 4.17 Hz. Hence, damage has caused a fundamental change in the internal damping force. This same behavior is observed for different input amplitudes and a similar behavior is observed in the stiffness restoring force.

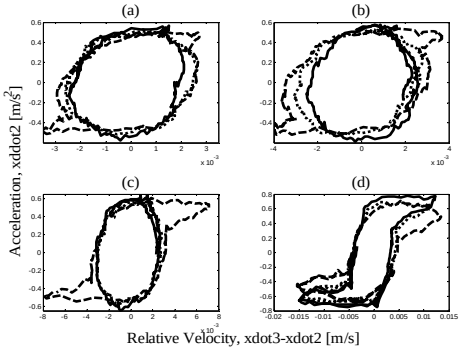

Fig 6: Change in frequency characteristic of damping internal force in the strut with damage. Bolt torques: 250 lb-in (——), 100 lb-in (····) and no bolt (– – –). Frequency: (a) 4.05 Hz, (b) 4.09 Hz, (c) 4.17 Hz and (d) 4.37 Hz. Input amplitude 0.5 mm.

It appears that the loosened bolt restricts the relative velocity, and increases friction, which causes the system to stay in the central hysterisis loop longer in terms of frequency. On the other hand, the lack of a bolt allows greater relative velocity and the characteristic of the force changes at a lower frequency. This fundamental change in the characteristic of the internal force of the system shows that restoring forces can be used as indicators of the presence of damage.

3.3 Frequency Domain Nonlinear ARX Models

Keeping the event-driven nature of the passive diagnostic algorithms in mind, the models were applied using random input data with a Gaussian distribution for various input amplitudes ranging from 0.5 mm to 6.0 mm RMS displacements of the wheel pan (i.e., tire patch of the Isuzu). The signal processing parameters are given in Tab. 2.

Table 2: Signal Processing Parameters for Random Input.

Time Points, N_t	Sampling Freq., F_s (Hz)	Number of Averages, N_{avg}	Over -lap	Window Type	LPF cut-off (Hz)
180,000	600	100	50%	Hanning	100

First, the 1st order, linear model in Eq. (5) was applied to the data, and the complex coefficients and damage features were estimated. For the damage induced by loosening the bolt connecting the steering knuckle to the control arm, Figs. 7-9 show the estimated exogenous coefficients and auto-regressive coefficients, $1-\left|A_j(\omega)\right|$ and $1-\left|A_{j_d}/A_{j_{un}}\right|$ for the vertical motion data from points x_2 and x_3, with x_3 taken as the input, *U(k)*.

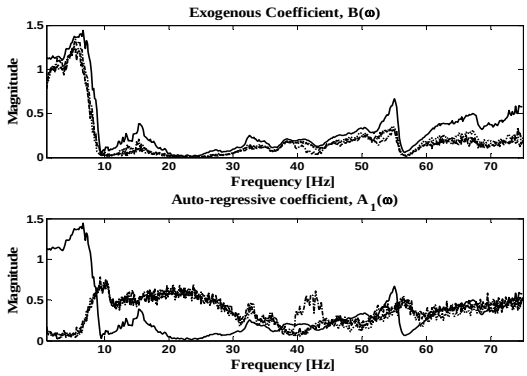

Fig 7: Exogenous and auto-regressive coefficients for linear model; Transmissibility function, T_{23} (——), for undamaged system at 400 lb-in torque; Coefficients for undamaged (····) and damaged cases, 100 lb-in (–.–.–) and no bolt (– – –).

Figure 7 shows the baseline transmissibility function, T_{23}, and the exogenous coefficients, $B(\omega)$, and auto-regressive coefficients, $A_1(\omega)$, for different bolt torques (damage). There are clear differences, with the most obvious in the 40-55 Hz range, where the 100 lb-in torque case**,** has less linear correlation and more nonlinear correlation than the other two cases. It can be seen that the undamaged case, and the case with no bolt, have very similar behavior. Another thing to note is that the nonlinear correlation is consistently higher for the damage cases above 60 Hz. As stated earlier, the quantity $1-\left|A_j(\omega)\right|$ is much like coherence. Figure 8 shows this quantity for the different bolt torques along with the ordinary coherence for the undamaged case. This quantity has the same form as the coherence and shows the same trend as highlighted before in the exogenous and auto-regressive coefficients, with the 100 lb-in torque case, showing greater nonlinearity in the 40-55 Hz range.

Figure 9 shows the quantity $1-\left|A_{j_d}/A_{j_{un}}\right|$. Any non-zero value shows a change in the auto-regressive coefficients and is an indicator of change in nonlinearity. It shows the same trend as before. The indicators discussed show that as the bolt is loosened, the nonlinearity in the path between x_2 and x_3 increases, due to the increased friction between the bolt and the ball joint caused by relative motion. The nonlinearity decreases when the bolt is removed as the source of the increased friction is no longer present. This is similar to the behavior observed in the restoring forces. The intermediate damage cases have different characteristics from the undamaged case and the most severe case (no bolt) behaves similar to the undamaged case.

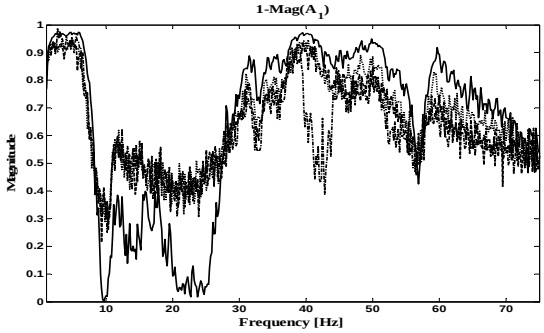

Fig 8: Ordinary Coherence (——) for undamaged system (400 lb-in torque); 1-Mag($A_1(\omega)$) for linear model at 400 lb-in (····) torque, 100 lb-in (–.–.–) torque and no bolt (– – –).

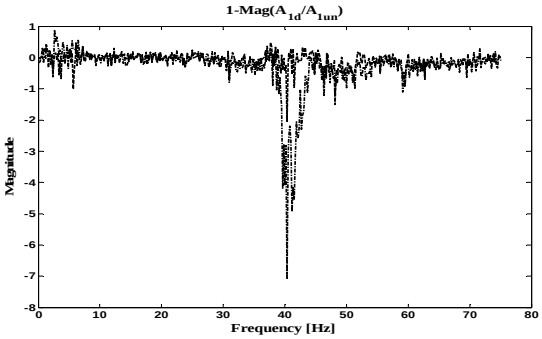

Fig 9: 1-Mag($A_{1d}(\omega)$/ $A_{1un}(\omega)$) for linear model; 100 lb-in torque (–.–.–) and no bolt (– – –).

The lateral direction data exhibits the same pattern but to a lesser extent than the vertical direction. The longitudinal direction shows the least change. The bolt axis was in the longitudinal direction, causing motion in the x-z plane due to loosening of the bolt; hence, those two directions show damage more clearly. Data from points along the path on which no damage is found gave no indication of damage. Hence, the damage has been located.

The 1st order, nonlinear model (Eq. (6)) was also applied to the data and the same trends were observed. The nonlinear correlations increase as the bolt is loosened and decrease when the bolt is removed completely. The auto-regressive coefficients show an interesting fact. Figure 10 shows that the super-harmonic frequency correlations are quite significant while there is almost no sub-harmonic correlation. This means that the third super-harmonic of the forced response of the system feeds back and acts as an internal input to the system (which is symptomatic of nonlinear behavior), while the third sub-harmonic does not. This is to be expected as these are forced harmonics rather than harmonic resonances, which would have sub- and supper-harmonic correlations. In the nonlinear model we are assuming than the nonlinearity is cubic in nature, hence, if the forcing function is harmonic (e.g., cos(ωt)) the cube of the function gives frequency components at the forcing frequency and the third multiple.

$$\left(\cos(\omega t)\right)^3 = \frac{3}{4}\cos(\omega t) + \frac{1}{4}\cos(3\omega t) \tag{9}$$

Equation (9) shows that there are no sub-multiple components. This equation explains why, in Fig. 10 there is no real correlation with the third sub-harmonic of the forcing frequency and extensive correlation with the third super-harmonic.

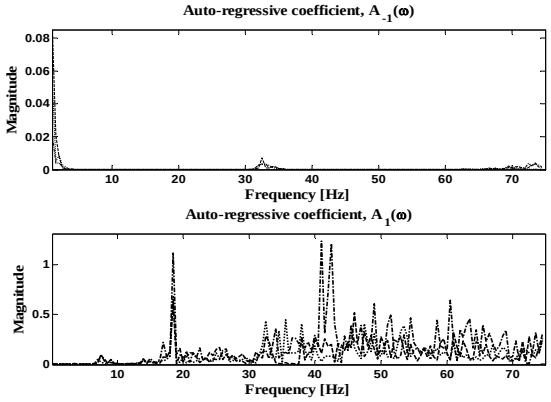

Fig 10: Auto-regressive coefficients $A_{-1}(\omega)$ and $A_1(\omega)$ for nonlinear model; 400 lb-in torque (····), 100 lb-in (–.–.–) and no bolt (– – –).

3.4 Experimental Sensitivity Functions

The data for this technique was collected from the Lexus using broadband random inputs similar to those used for the ARX models. In the absence of load cells on the hydraulic shaker apparatus, the fundamental mechanics model, Fig. 1, was used to estimate the force input to the spindle from the tire. The equation of motion of the unsprung mass, M_1, can be written as

$$\begin{aligned} &M_1\ddot{x}_1 + C_2\dot{x}_1 - C_2\dot{x}_2 + K_2x_1 - K_2x_2 \\ &+ N_1[x_1(t), x_2(t), \dot{x}_1(t)\dot{x}_2(t)] \\ &+ N_2[x_1(t), x_b(t), \dot{x}_1(t)\dot{x}_b(t)] \\ &= C_1(\dot{x}_b - \dot{x}_1) + K_1(x_b - x_1) \end{aligned} \tag{10}$$

The terms on the right hand side can be thought of as the inputs to the spindle (unsprung mass), F_1, due to the motion of the tire patch. In order to estimate the force, an accelerometer was placed at the wheel pan of the shaker to estimate the acceleration of the tire patch, $\ddot{x}_b$. The stiffness of the tire, K_1, was estimated using a static deflection test. The stiffness was estimated to be about 1000 lb/in, which is the value for a typical passenger car in the USA. The damping, C_1, was assumed to be 1/100th of the stiffness, i.e., 10 lb-s/in, although it was observed that damping did not have a significant effect on the results. In order to estimate the sensitivity of H_{11} (driving point FRF of unsprung mass) to the stiffness between locations x_1 and x_3, K_{13}, Eq. (7a) was used.

$$\frac{\partial H_{11}}{\partial K_{13}} = -\left[H_{11} - H_{13}\right]^2 \tag{11}$$

Then Eq. (8a) was used to estimate the change in the stiffness K_{13} with each incremental change in preload. It should be noted that the experimental sensitivity, Eq. (11), has to be evaluated for each different preload because the system parameter, K_{13}, has changed.

For each change in bolt torque (preload), the finite difference, ΔH_{11}, and the experimental sensitivity, Eq. (11), was estimated and the change in stiffness was estimated from Eq. (8a). The location of the bolt on the Lexus suspension was such that it could not be accessed with a torque wrench and, hence, the torque could not be measured. The bolt was first loosened by half a turn, then three turns and finally removed completely. Figure 11 shows the estimates of experimental sensitivity (Eq. (11)), ΔH_{11} and ΔK_{13} for the first change in bolt preload, half turn. The experimental sensitivity and finite difference have a similar shape and, hence, ΔK_{13} is reasonably constant over most of the frequency range of interest. The estimated value of ΔK_{13}, from the 5-10 Hz range, is 5,373 lb/in. Figure 12 shows the estimated values of ΔK_{13} for the different bolt preloads, showing fairly constant values over the 5-15 Hz range. The change in stiffness for loosening of the bolt by three further turns is 12,613 lb/in and the change for removing the bolt completely is 2,134 lb/in. Thus, the damage has been quantified as it progresses.

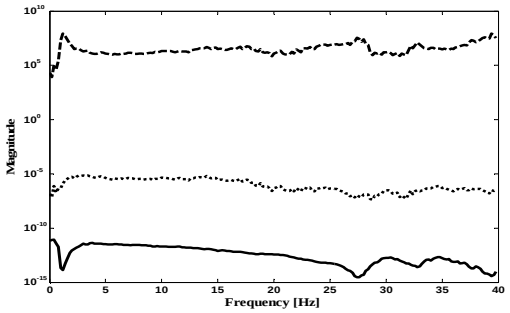

Fig 11: Experimental Sensitivity (——), finite difference, ΔH_{11}, (····) and estimated change in stiffness, ΔK_{13}, (– – –), for loosening of the bolt by a half turn.

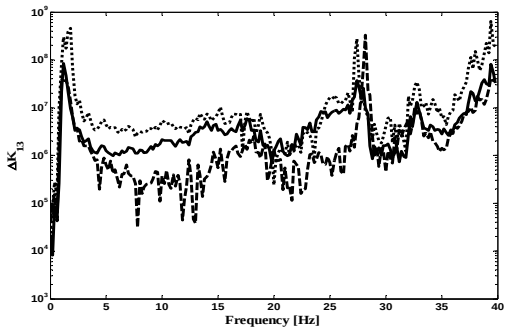

Fig 12: ΔK_{13} for changes in bolt preloads, half turn (——), three turns (····) and no bolt (– – –).

4 CONCLUSIONS

Two passive methods and one active vibration-based method for damage identification were presented in this paper. The two passive techniques are restoring forces and transmissibility-based frequency domain ARX models, which use response acceleration measurements to detect and locate damage. Restoring force curves map changes in internal restoring forces caused by changes in system parameters (linear and nonlinear) due to damage, while ARX models track the changes in linear and nonlinear frequency correlations with the progression of damage. The use of transmissibility (output-only) formulation allows the damage to be located, due to the increased sensitivity to local system dynamics as compared to global dynamics. The preferential frequency bandwidth of the two passive techniques, narrowband for restoring forces and broadband for ARX models, motivates the selection of the algorithms in an event-driven manner based on the observed frequency bandwidth of the response.

The active technique uses experimental sensitivity functions to detect, locate and quantify damage by comparing the sensitivity functions to finite difference approximations of the change in system FRFs due to damage. The techniques were applied to experimental vehicle data, and the damage introduced by loosening of bolts was detected, located and quantified.

ACKNOWLEDGMENTS

The authors would like to thank ArvinMeritor and the Center for Advanced Manufacturing at Purdue for their technical and financial support of this research.

REFERENCES

[1] Doebling, S.W., Farrar, C.R., Prime, M.B. and Shevitz, D.W., 1996, "Damage Identification and Health Monitoring of Structural and Mechanical Systems from Changes in Their Vibration Characteristics: A Literature Review," Los Alamos National Laboratory Report, LA-13070-MS.

[2] Doebling, S.W., Farrar, C.R., Prime, M.B. and Shevitz, D.W., 1998, "Review of Damage Identification Methods that Examine Changes in Dynamic Properties," Shock and Vibration Digest, **30(2)**.

[3] Rytter, A., 1993, "Vibration Based Inspection of Civil Engineering Structures," Ph.D. Dissertation, Department of Building Technology and Structural Engineering, Aalborg University, Denmark.

[4] Masri, S.F., Caughey, T.K., Miller, R.K., and Saud, A.F., 1987, "Identification of Non-Linear Vibrating Structures: Part I – Formulation," Journal of Applied Mechanics, **54**, pp. 918-922.

[5] Masri, S.F., Caughey, T.K., Miller, R.K., and Saud, A.F., 1987, "Identification of Non-Linear Vibrating Structures: Part II – Applications," Journal of Applied Mechanics, **54**, pp. 923-929.

[6] Haroon, M, Adams, D.E., Luk, Y.W. and Ferri, A.A, 2005, "A Time and Frequency Domain Approach for Identifying Non-Linear Mechanical System Models in the Absence of an Input Measurement," Journal of Sound and Vibration, **283**, pp. 1137-1155.

[7] Adams, D.E. and Allemang, R.J., 2001, "Discrete Frequency Models: A New Approach to Temporal Analysis," Journal of Vibration and Acoustics, **123**, pp. 98-103.

[8] Adams, D.E., 2002, "Frequency Domain ARX Model and Multi-Harmonic FRF Estimators for Non-Linear Dynamic Systems", Journal of Sound and Vibration, **250(5)**, pp.935-950.

[9] Adams, D.E. and Farrar, C.R., 2002, "Classifying Linear and Non-Linear Structural Damage Using Frequency Domain ARX Models," Structural Health Monitoring, **1(2)**, pp.185-201.

[10]Zhang, H., Schulz, M. J., Naser, A., Ferguson, F., and Pai, P.F., 1999, "Structural Health Monitoring Using Transmittance

Functions," Mechanical Systems and Signal Processing, **13(5)**, pp. 765-787.
[11] Johnson, T. J. and Adams, D. E., 2002, "Transmissibility as a Differential Indicator of Structural Damage", American Society of Mechanical Engineering Journal of Vibration and Acoustics, **124(4)**, pp. 634-641.
[12] Yang, C., Adams, D.E., Yoo, S.-W., Kim, F.-J., 2003, "An Embedded Sensitivity Approach for Diagnosing System-Level Vibration Problems," Journal of Sound and Vibration, **269(3-5)**, pp. 1063-1081.
[13] Johnson, T.J., Yang, C., Adams, D.E. and Ciray, S., 2005, "Embedded Sensitivity Functions for Characterizing Structural Damage," Smart Materials and Structures, **14**, pp. 155-169.